Glass Struct. Eng. (2017) 2:79–101
DOI 10.1007/s40940-016-0033-2

RESEARCH PAPER

Laminated connections for structural glass components: a full-scale experimental study

Manuel Santarsiero · Christian Louter · Alain Nussbaumer

Received: 1 April 2016 / Accepted: 14 June 2016 / Published online: 8 July 2016

Abstract The use of glass material for structural components has drastically increased in the last decade. Among others, a laminated connection is a type of adhesive joint that makes use of foil interlayer adhesive to transfer forces between glass and metal parts. In this work, the use of embedded laminated connections is studied as connection between glass beams. In particular, it is experimentally investigated the use of embedded connections laminated to make a moment joint between laminated glass beam segments. The mechanical behaviour of such glass beams with embedded laminated connections is studied under different loading scenario. Tests are performed under monotonic, creep and damage protocol. Different geometry and location of the embedded laminated connections are compared. The results of this work showed that embedded laminated connections represent an efficient means of load transfer between glass beams. It is observed that the choice of an appropriate geometry and location of the embedded connections can provide a substantial enhancement to the mechanical behaviour of the beam. In particular, a redundant and ductile structural behaviour of the moment connection can be achieved. Furthermore, results also showed that beams with embedded laminated connections are able to resist to severe damage scenarios and to sustain the applied load over time, even in the case of breakage of all glass panels.

Keywords Laminated embedded connections · Adhesive connections · Structural glass components · Experimental investigation · Mechanical behaviour · Redundancy · Ductility

M. Santarsiero (✉)
Eckersley O'Callaghan Engineers (EOC), London, UK
e-mail: manuel.santarsiero@gmail.com

M. Santarsiero · A. Nussbaumer
Steel Structures Laboratory (ICOM), School of Architecture, Civil and Environmental Engineering (ENAC), École Polytechnique Fédérale de Lausanne (EPFL), Lausanne, Switzerland
e-mail: alain.nussbaumer@epfl.ch

C. Louter
Department of Architectural Engineering and Technology (AE+T), Faculty of Architecture and the Built Environment (A+BE), Delft University of Technology (TU Delft), Delft, The Netherlands
e-mail: Christian.Louter@TUDelft.nl

1 Introduction

The use of glass material for structural components in building has drastically increased in the last decade. Due to the fragile nature of this material, connections between structural glass components represent one of the main critical aspects of glass engineering (Amadio et al. 2008; Baitinger 2009; Beyer and Seel 2012; Beyer 2007; Maniatis 2006; Mocibob and Belis 2010; Mocibob 2008; Overend and Maniatis 2007; Overend et al. 2013; Siebert and Herrmann 2010; Watson et al. 2013). This is because glass cannot plastically redistribute the stress peaks occurring where forces are transferred between components. Bolted connections

represent the most common solution to transfer load between glass components. However, a bolted connection requires the glass to be drilled, a process that often reduces the glass strength at the perimeter of the bore hole. In bolted connections, forces are locally transferred from bolt to glass. Although intermediary materials are used to spread the force, high stress intensification occurs at the perimeter of the bore hole. Because of these issues, adhesive connections have been used and studied in the last years as connections for structural glass applications (Belis et al. 2012; Blandini 2010; Dias et al. 2012; Dispersyn et al. 2015a, b; Dispersyn and Belis 2016; Dispersyn et al. 2014; Huveners et al. 2007; Ludwig 2014; Marinitsch et al. 2014; Marinitsch et al. 2015; Martens et al. 2016; O'Callaghan and Coult 2007; O'Callaghan 2009; Santarsiero et al. 2013a, b, 2014; Schneider and Franz 2012; Silvestru and Englhardt 2014; Vogt 2009; Watson 2010; Weller et al. 2011, 2012).

Among others, a laminated connection is a type of adhesive connection that makes use of an interlayer foil adhesive to transfer forces between glass and metal parts. The main concept of laminated connections is to use the same production process of laminated glass to make adhesive transparent connections. A solid foil of transparent adhesive material is placed between a metal connector and glass panel. Metal, adhesive and glass are then placed in a vacuum bag and subjected to the autoclave process of laminated glass. At the end of the lamination process the result is a glass component, in which the metal part is fully bonded to the glass plate via the transparent interlayer adhesive. Several authors have tested embedded connections with small-scale test (Belis et al. 2009; Carvalho et al. 2011; Carvalho and Cruz 2012; Lenk and Lancaster 2013; Ludwig 2015; Puller et al. 2011; Puller and Sobek 2012; Puller 2012; Santarsiero and Louter 2013; Santarsiero et al. 2013a; Santarsiero 2015). However, limited information is available in literature on the behaviour of large-scale glass components with embedded connections.

In this work, the use of laminated connections between glass beams is investigated. In particular the use of embedded connections to make a moment joint between laminated glass beams is studied. This connection could represent, in terms of practical application, either a beam-to-beam, or beam-to-fin or fin-to-fin connection.

The aim of this work is to (i) investigate with large-scale tests the structural performance of embedded connections as means of moment transfer between beams (ii) to compare the performance of different types of embedded connections in beams (iii) to evaluate the creep response under constant load and (iv) to study the effects of a accidental scenario of vandalism damage of a beam with embedded connections under constant load over time.

Different types of tests are performed and the results are analysed and discussed in this paper. Three types of embedded connections with different geometries and positions in the beam are investigated. Three different testing protocols are used: monotonic loading, creep loading and damage infliction under constant load. The materials and the geometries of the tested specimens are presented in detail in Sect. 2. The test methodology, measurements and load protocols are described in Sect. 3, while the tests results are collected in Sect. 4. Analysis and discussion of the results are then presented in Sect. 5. The conclusions and outlook derived from this work are finally given in Sect. 6.

2 Materials

In this work, 3 m glass beams composed of laminated glass panels are investigated. Each laminated component is made of three glass panels of nominal thicknesses 6–10–6 mm. The glass panels are laminated with 1.52 mm foil of SentryGlas® ionomer interlayer. The glass beams are reinforced with 3 mm stainless steel (316 L) bars, at the top and bottom edge of the laminated glass. This is because the goal of these tests is to investigate the behaviour of beams with embedded connections, with particular focus on the behaviour at the connection region. The use of reinforcement bar would avoid that a bending crack occurring far from the connection would result in the interruption of the test. The steel bars are bonded to the beam edges with SentryGlas® interlayer (Fig. 1).

The 3 m beams are composed of two laminated glass beam segments (nominal dimension 1500×300 mm) with a moment connection in the centre (see Fig. 4). In the following paragraphs, with 'beam', it is therefore intended a three-meter glass component composed by two 1.5 m 'beam segments'. The moment connection in the centre is made by embedded laminated connections. More specifically, embedded metal inserts are laminated into the glass to transfer the forces between the beam segments.

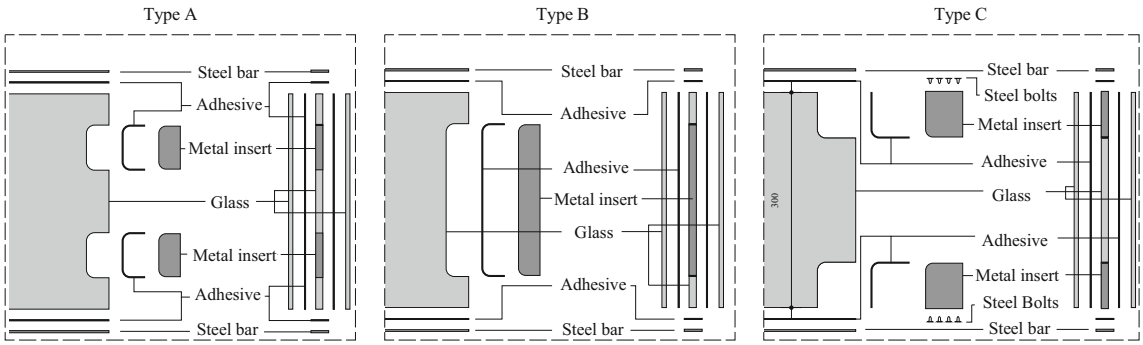

Fig. 1 Exploded schemes of beam type A–C

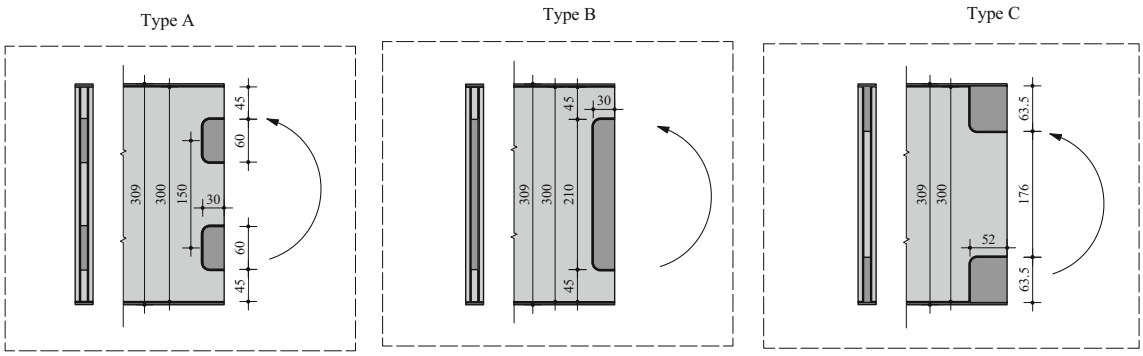

Fig. 2 Dimensions and locations of the metal inserts in beam type A–C

Three different types of beams are tested. Each type has different location and geometry of the metal inserts: type A with the inserts located at an intermediate position, type B with a single, yet extended insert located at the centre, and type C with the inserts located at top-bottom position. Furthermore, in type C, the metal inserts are connected to the stainless steel reinforcement bars, as elucidated at the end of this section. Figure 2 shows the location and the dimensions of the metal inserts. In the following paragraphs, 'type A beam' therefore indicates a glass beam with type A connection, and so on.

To fabricate laminated connections, a recess is made in the inner glass panels. The recess in the glass is made with a numerically controlled machine (CNC processing). All edges of the glass panels are polished, including the edges of the recess. SentryGlas® interlayer of 1.52 mm thickness is placed between metal insert and the glass edge.

The metal inserts are made of 316 L stainless steel. The thickness of each metal insert is 10 mm, same as the nominal thickness of the inner glass plate. The dimensions of the metal insert are: 60×30 mm for type A, 210×30 mm for type B and 63.5×52 mm for type C. The dimension of the metal insert is based on previous work on small scale testing in (Santarsiero 2015). The fillet radius of the metal inserts at the corners is 10 mm. Each face of the insert is polished to R = 0.8 micron. In this paper, the following definitions are used to indicate the faces of the metal insert (see also Fig. 3): lateral faces (the two large lateral face), lateral edge (10 mm wide edge parallel to long horizontal dimension of the beam) and frontal edge (10 mm wide edge orthogonal to the long horizontal dimension of the beam). The embedded metal inserts are bonded to the glass plates by SentryGlas® adhesive at the two lateral faces and at the edges. In addition, type C metal inserts are also connected to the steel bars with 4 M6 bolts, class 12.8.

Fig. 3 Definitions of the surfaces of the metal insert

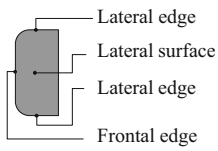

The metal inserts of the two beam segments are then connected with solid pieces of mild steel S355 and M8

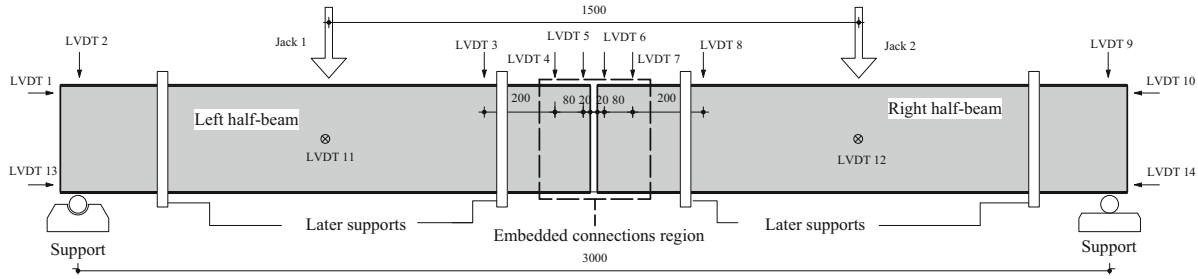

Fig. 4 Plan of the test setup

bolts. Class 12.8 bolts are used to prevent yielding of the bolts during the test, due to the high force to be transferred.

3 Methods

This section describes the testing methodology and protocols used in this work to test the mechanical performance of glass beams with embedded connections, with different geometries and subjected to different loading conditions and scenarios. In the following one test per each configuration it is performed.

Type A–C beams are investigated under four point bending tests (4PBT) (see Figs. 4 and 5). The beams are subjected to a uniform bending field distribution between the two central forces, i.e. in the centre of the beam. The distance between the two forces is 1500 mm.

The beams are spanning between two supports at a distance of 3000 mm. Each support is made of two concrete blocks with steel cylinder bearings located on top. The two bearings allow for free rotation of the beam-ends. The left bearing allows also for horizontal displacements. The out-of-plane movement of the beam is restrained by four lateral supports. PTFE plates are placed between the lateral supports and the beam to ensure friction-less vertical movement during the test.

Two 150 kN hydraulic jacks are used to apply the two vertical forces indicated. Two 150 kN electrical load cells are then placed between jacks and the beam to measure applied force during the tests.

Vertical and horizontal displacement of the beam is measured by means of LVDTs. The location of the LVDTs is schematically shown by Fig. 4. LVDTs positioned along the top beam edge are used to measure the vertical displacements at different points of the beam. The vertical LVDTs at the two supports are used to

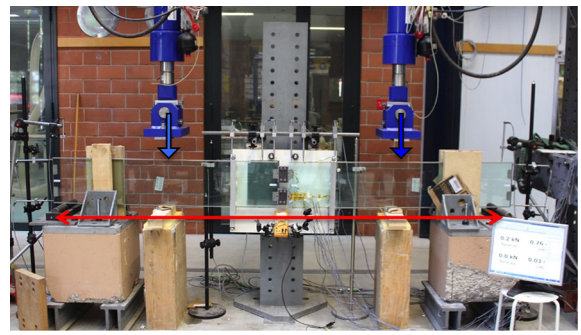

Fig. 5 Photo of the test setup

compensate for setup deformation. Although the lateral displacement is restricted by the lateral supports, the lateral displacement is monitored by means of LVDTs horizontally placed at position 11 and 12 (not here presented for the sake of brevity), see Fig. 4. All measurements are recorded at a frequency of 10Hz.

Strain gauges are used to measure the strain field distribution on the external glass surfaces during the test. Additional compensation strain gauges are glued on an additional unloaded reference laminated glass panel (with same thickness 6–10–6 mm) to compensate for strain variations due to temperature fluctuations. Figure 6 shows a scheme of the strain gauges locations. The strain gauges indicated as 'middle gauges' and 'connection gauges' are glued on both faces of the beams and average values are calculated. All strain gauges measurements are collected in Appendix A.

The beams are tested using three different loading protocols: monotonic, creep and damage test. All tests are performed at temperature equal to 26 ± 2 °C (laboratory condition). Table 1 collects an overview of the beams composition for each test.

Firstly, the beams are tested under monotonic loading. Tests are conducted in displacement control. The

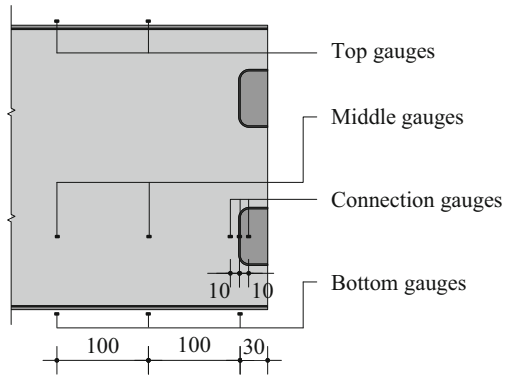

Fig. 6 Location of the strain gauges used in the test on for type A and B. Type C is identical with 'connection' and 'middle' gauges located at 20 mm from bottom glass edge. Top and bottom gauges are glued on the steel bars

displacement rate is 0.01 mm/s. This rate is chosen bases on practical limitation. One of the two jacks is driven in displacement control. The second one is set to apply the same load of the other jack (load control regime). This allows to compensate for tolerances and ensures a symmetric load application. Monotonic tests are performed on type A, B and C beams. Glass panels are annealed. Annealed glass is used because fracture pattern of annealed glass lets to analyse the stress distribution in the glass and to provide a mechanical interpretation to the structural behaviour of the beams at the connections.

Secondly, a creep-loading protocol is used to investigate the mechanical response of the beams over time. More specifically, the beams are subjected to constant load over time set to 50 % of the load at glass breakage from the monotonic tests. Creep displacements and deformations are measured over time. Creep tests are performed on type A–C beams. Glass panels are annealed. The duration of the creep test is 360 min for type A and C beams. Creep test of type B was 250 min because of practical limitation.

Thirdly, the response to an accidental vandalism scenario is investigated. This protocol consists in damaging a type C glass beam subjected to constant load over time. The aims of this test are to (i) simulate a scenario of vandalism damage with sharp objects (ii) to investigate the effects of such damage to the beam subjected to constant load over time and (iii) evaluate the level of redundancy and post-fracture performance of type C beam in case of severe damage scenario. In order to maximise the effects of an inflicted damage, the beam used for this third protocol is composed by a fully tempered (FT) beam segment on the left and a heat-strengthened (HS) beam segment on the right. Residual tempering stresses are measured to be 102 ± 1 MPa for the external layers of the FT beam segment and 51 ± 1 MPa for the external layers of the HS beam segment. Measurements are made with SCALP-05.

In this last protocol, the beam is firstly loaded in displacement control up to 50 % of the load at glass breakage. Loading jacks are set in load control regime, i.e. constant load over time is applied regardless the beam response. Then, the two external layers of the FT beam segment are broken and the effects of breakages are reordered over time. The beam is left under constant load over 18 h and displacements are recorded over time. After this stage, the other HS beam segment is damaged with a sharp hammer. Glass fragmentation is induced by manually hitting the beam with at sharp metallic hammer in several locations along the beam. Load is kept constant and the response is measured over time. Finally, the third and last inner layer of the tempered beam segment is broken and load is kept constant over time.

Table 1 Overview of the composition of the glass beams tested with different protocol

Test	Load protocol	Left beam segment	Right beam segment	Connection type
1	Monotonic	Annealed	Annealed	A
2	Monotonic	Annealed	Annealed	B
3	Monotonic	Annealed	Annealed	C
4	Creep	Annealed	Annealed	A
5	Creep	Annealed	Annealed	B
6	Creep	Annealed	Annealed	C
7	Damage	Fully tempered	Heat-strengthened	C

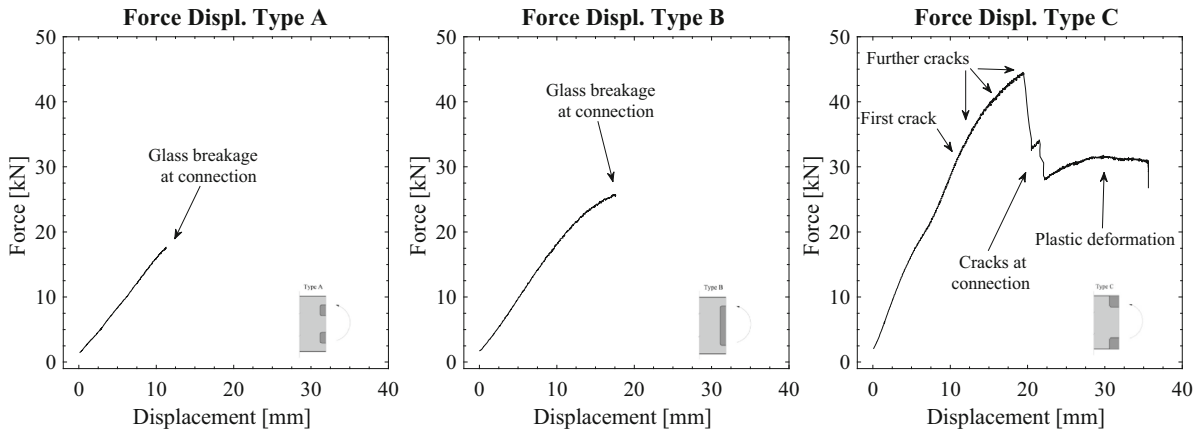

Fig. 7 Load-displacement curves from monotonic tests: **a** type A, **b** type B and **c** type C

4 Results

This section presents the test results of beams with embedded laminated connections at different locations, with different geometries and subjected to different loading protocols. Monotonic test results are shown first. Then, the results of creep tests are presented. Finally, the test results of beam subjected to a damaging scenario are described. Analysis and discussion of the results are then presented in the following Sect. 5.

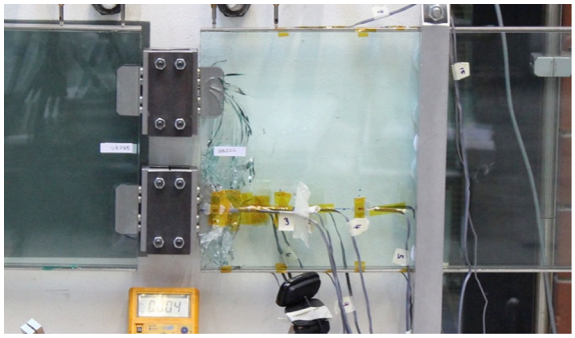

Fig. 8 Photo of type A beam after monotonic test

4.1 Monotonic test results

This section presents the results of the monotonic tests. Figure 7 shows the load displacement curves for the three types of beams. With load is intended the sum of the two forces applied by the jacks. With displacement is intended the displacement of the beam in the centre, computed as average of LVDTs number 5 and 6 (see Fig. 4). Beams are loaded up to failure in displacement control. In the following paragraphs, with *breakage* is intended the occurring of cracks in the glass panels, while with *failure* is intended the ultimate displacement capacity of the beam.

Type A showed a linear behaviour up to failure (Fig. 7a). Failure is occurring at a maximum load of 17.5 kN and it is due to glass breakage. No major delamination or glass cracking is observed before reaching the maximum force. The cracks in the glass are mainly localized at the connection region (see Fig. 8). More specifically, the fracture pattern is highly concentrated at the bottom connections. Further analyses of the fracture pattern are provided in Sect. 5.

Type B beam initially shows a linear elastic behaviour as for type A. Then, the force displacement curve deviates from linearity approximately at 22 kN. The test continued showing non-linear response up to failure. Failure is occurring at a maximum load of 25.5 kN due to glass breakage. No major delamination or glass cracking is observed before reaching the maximum load. The glass cracking is mainly localized at the connection (see Fig. 9). More specifically, the fracture pattern is highly concentrated at the bottom of the connections. Further analyses of the fracture pattern are provided in Sect. 5.

Type C beam shows a different mechanical behaviour than type A and B. The load displacement curve initially exhibits a linear elastic response. A first glass crack is occurring at 32.4 kN. This crack does not affect the load displacement curve, which shows a continu-

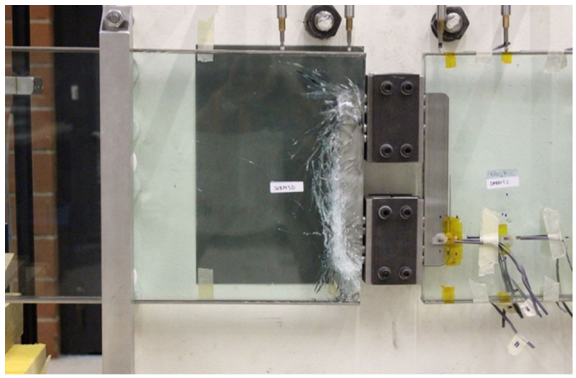

Fig. 9 Photo of type B beam after monotonic test

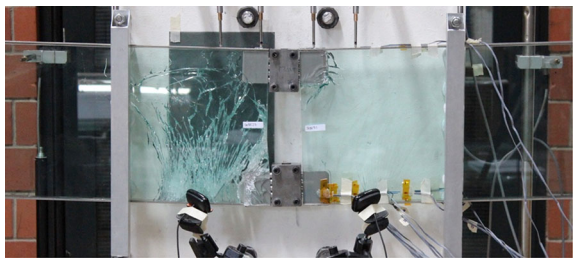

Fig. 10 Photo of type C beam after monotonic test

ous behaviour without mayor discontinuity. The crack is occurring in a region far away from the connection. More specifically, the crack is occurring at the bottom edge of the beam. The crack is located in one layer only of the laminated beam, i.e. does not go through all glass layers. After the first crack, the load increases linearly with increasing displacement. Then, further cracks occur without effects in the load displacement curve. At this stage the crack appears to not overlap each other. At approximately 40 kN the curve deviates from linear trend. At the maximum load, equal to 44.5 kN, more severe cracks occur through each layer of the glass beam (i.e. overlapping over the three layers) and the load drops down to 32.5 kN. At this stage, all cracks are concentrated in a region far from the connection. The load then increases again until more cracks occur and load drops to 28 kN. These new cracks are located at the connection region. At this stage, both beam segments are severely cracked (Fig. 10). The test proceeds and, with the increasing of displacement, the load increases further. Large displacements are then observed with a plastic plateau occurring at approximately 31.5 kN. The beam failure is finally reached at 35.6 mm of displacement due to the breakage of the reinforcement on

Fig. 11 Photo of type C beam at connection after monotonic test

the left beam segment. Figure 11 shows a photo of the crack pattern at the connection after test.

4.2 Creep test results

As described before, the beams investigated in this paper make use of laminated connections to transfer load between the two beam segments. The metal inserts are bonded to glass plates by the interlayer adhesive. Since SG exhibits a visco-elastic behaviour, it is expected to observe creep deformation over time when a beam is subjected to constant load. Because of this reason, type A–C beams are subjected to creep test and the response over time is measured. More specifically, beams are subjected to constant load over time and displacements are recorded.

Figure 12 shows the load applied by the hydraulic jacks over time under load control protocol. It can be seen that the hydraulic jacks apply an approximately constant load over time with minor fluctuation. Figure 13 shows that these fluctuations have minor effect on the mechanical response of the beams. Indeed, the measured displacements have a continuous behaviour without discontinuities.

Figure 13 shows displacement over time for the three types of beams. At the beginning, when load is applied, all three beams show a linear response to the application of load. Then, when load is kept constant over time, the displacement increases over time, i.e. the beams creep over time. In particular, for beam type A displacement goes from 6.8 to 7.9 mm, for beam type B displacement goes from 5.3 to 7.0 mm and for beam type C displacement goes from 5.1 to 5.6 mm.

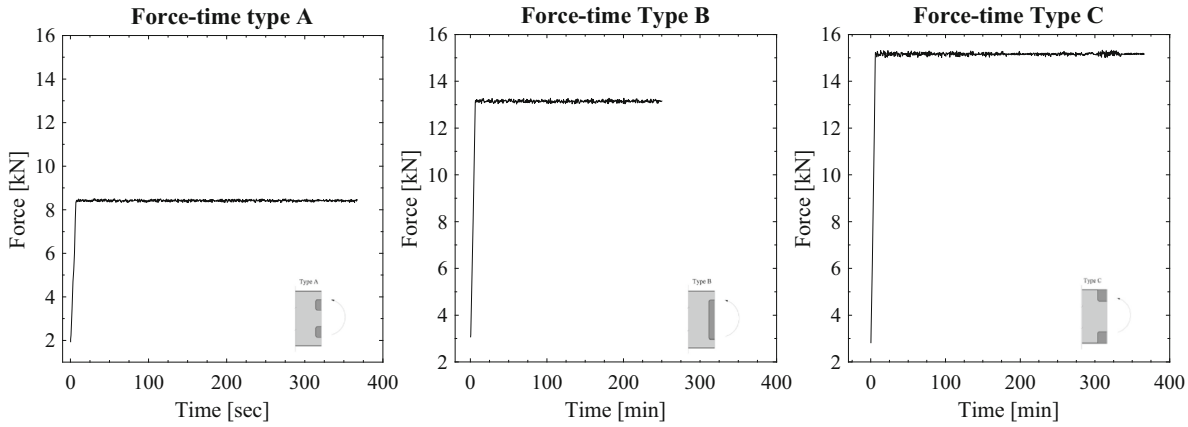

Fig. 12 Results of creep tests: load versus time in load control regime of **a** type A, **b** type B and **c** type C

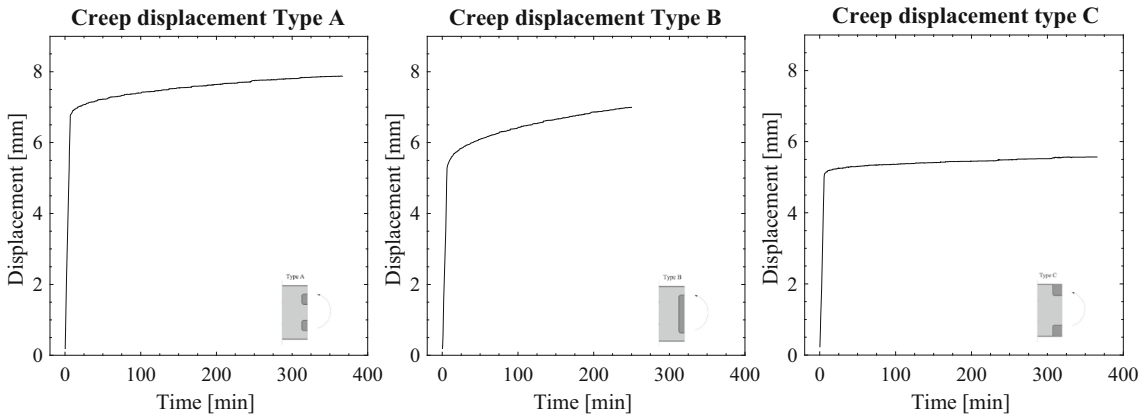

Fig. 13 Results of creep tests: displacement versus time under constant load of **a** type A, **b** type B and **c** type C

4.3 Damage tests results

This section presents the test results of a type C beam that is intentionally damage under constant load over time. In the following paragraphs, with *damage*, it is intended one or more cracks in the glass are intentionally induced with a sharp metallic object. In this test, tempered glass is used for the left beam segment and HS glass for the right beam segment. This is done to maximize the effect of intentionally induced damage.

A type C beam is firstly loaded up to 15 kN and load is kept constant over time. The loading jacks are set in load control regime, i.e. they apply the set load regardless the mechanical response and stiffness changes (e.g. due to breakage) of the beam. After a short period of time, damage is manually induced to the left beam segment. More specifically, a metallic hammer is used to crack the two external layers of the left beam segment (see Fig. 14). Because the panels are FT, cracks immediately propagate entirely over both glass panels (see Fig. 15). This is because of the high strain energy stored in the glass panel due to the high residual stress induced by the thermal tempering process.

Full fragmentation of the external panels does not induce collapse of the beam. However, the fragmentation has an effect on the mechanical response of the beam. More specifically, the vertical displacement increases with approximately 0.7 mm after the fragmentation (see Fig. 16b). More detailed analyses are given in the following Sect. 5. After the damage, the beam is kept under constant load over 1080 min (18 h). The vertical displacements over time during this creep phase are shown in Fig. 16b. It is observed that the displacement over time goes from 5.0 to 7.0 mm. It should

Fig. 14 Glass beams during damage with metallic hammer (see *left* side of beam)

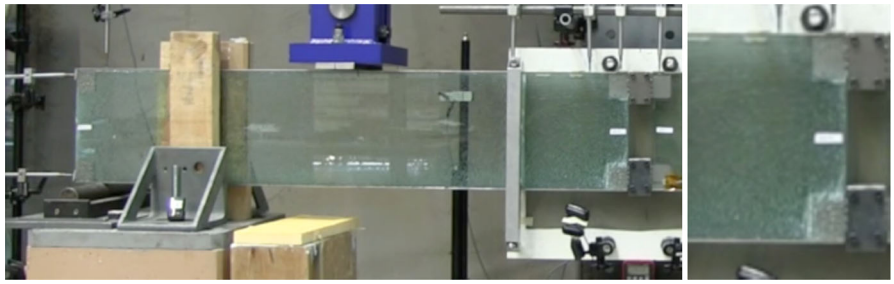

Fig. 15 Full breakage of 2 out of 3 FT glass layers (outer) of type C beam under constant load

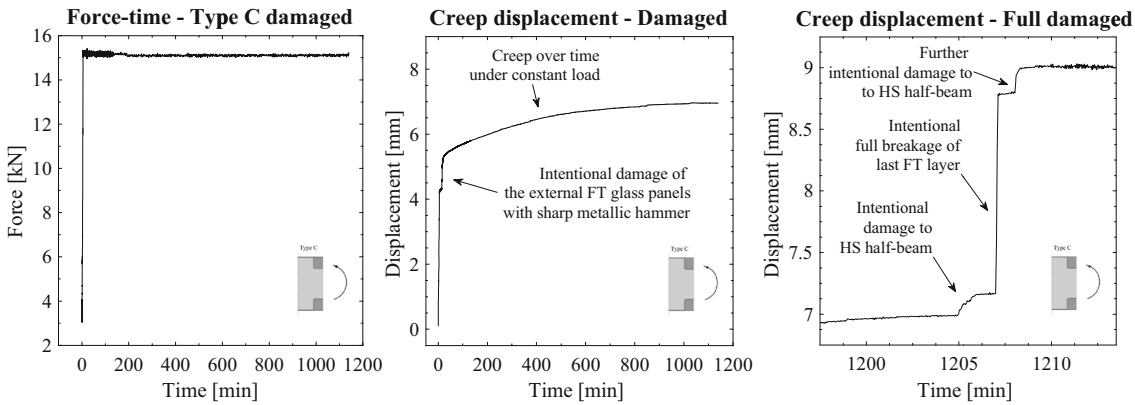

Fig. 16 Damaged type C beam **a** applied force over time, **b** creep displacement over time after breakage of 2 FT glass panels and **c** displacement after further damage of the beam

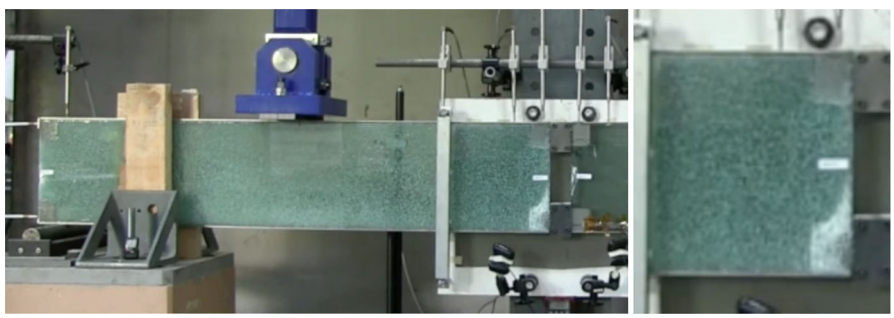

Fig. 17 Full breakage of 3 out of 3 FT glass layers of type C beam under constant load

be noticed that, at this stage of the test, the left beam segment has two out of three layer fully cracked. The small fragments of broken glass are kept in place by the adhesive laminated interlayer.

The beam is then subjected to further damage (see Fig. 17). Firstly the right HS beam segment is damaged. This is done by inducing cracks at the two vertical short edges of the beam segment, i.e. the edge at

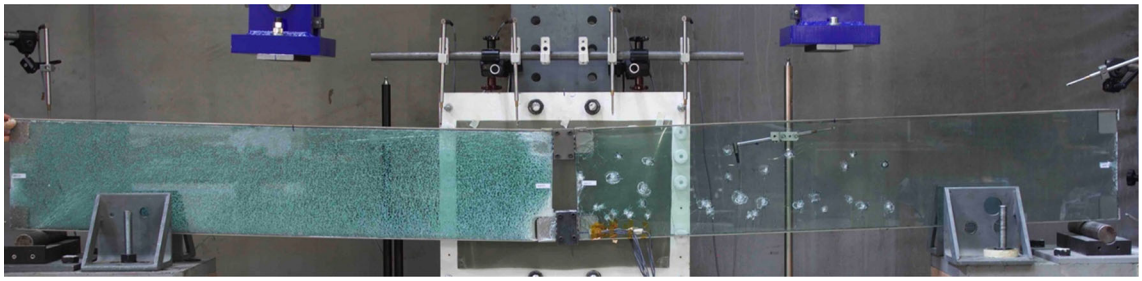

Fig. 18 Type C beam after damage test

the support and the edge at the connection. Because of the residual stress of HS glass panel, the cracks propagate throughout the beam segment. The vertical displacement increases from 7.0 to 7.2 mm (see Fig. 16c). Then, the inner layer of left FT beam segment is broken. The cracks propagate and the whole panel is cracked in small pieces because is FT. At this stage, the left beam segment glass is fully broken, i.e. each layer of the left beam segment is fully fragmented. The displacement further increases from 7.2 to 8.8 mm.

Finally, more severe damaging is induced to the right beam segment. This is done hitting the beam with a sharp metallic hammer in several locations (see Fig. 18). This further damage does not cause to the collapse of the beam but rather an increase of vertical displacement, which increases from 8.8 to 9.0 mm. Since none of the induced damage caused collapse of the beam, a final monotonic test is performed, which showed identical behaviour to the previous monotonic test (not here presented for the sake of brevity).

5 Analysis and discussion

5.1 Monotonic tests

5.1.1 Type A and B beams

Figure 19a, b shows the crack pattern of the type A beam after monotonic test. Different considerations can be made from the fracture patter. Firstly, it is observed that the crack pattern at the bottom connection is different from the one at top connection. At the bottom, the cracks are more dense and in general vertically oriented. At the top, instead, the cracks are less dense and horizontally oriented. A possible interpretation can be derived from solid mechanics. In brittle material like glass, cracks are usually occurring orthogonal to principal tensile direction[1] (see Fig. 20a). By definition, cracks are therefore expected to occur orthogonal to principle tensile stresses and aligned to compressive stresses.[2]

Due to the bending moment transferred between the two beam segments, bottom and top inserts are subjected to tensile and compressive forces respectively (see Fig. 20b and c). The cracks are therefore expected to be in general vertically oriented at bottom connection while horizontally oriented at top connection, which is in line with the experimental observation (Fig. 19a, b). Between bottom and top insert there is a transition region. In this region, the bottoms vertical cracks curve towards horizontal direction along the direction of the compressive force.

The crack pattern at the bottom connection appears to be rather complex and further analysis is needed to provide a mechanical interpretation. The behaviour of an embedded connection can be decomposed in two systems: in-plane and through-thickness stress distribution. The in-plane behaviour can be described by the equilibrate strut-and-tie system shown by Fig. 19c. The force applied to the metal connection is transferred to the glass by horizontal and inclined tensile elements (horizontal elements located at the frontal edge and the 45° inclined at the two lateral edges. These tensile elements are then equilibrated by vertical and inclined compressed elements. According to the aforementioned consideration on brittle materials, the cracks are therefore expected to be oriented along the directions of the compressed elements, i.e. vertically along

[1] Following maximum stress failure criteria such as Rankin.

[2] A complete interpretation of location and orientation of crack involve a more extended consideration of the three-dimensional second order stress tensor, which is not here presented for the sake of brevity.

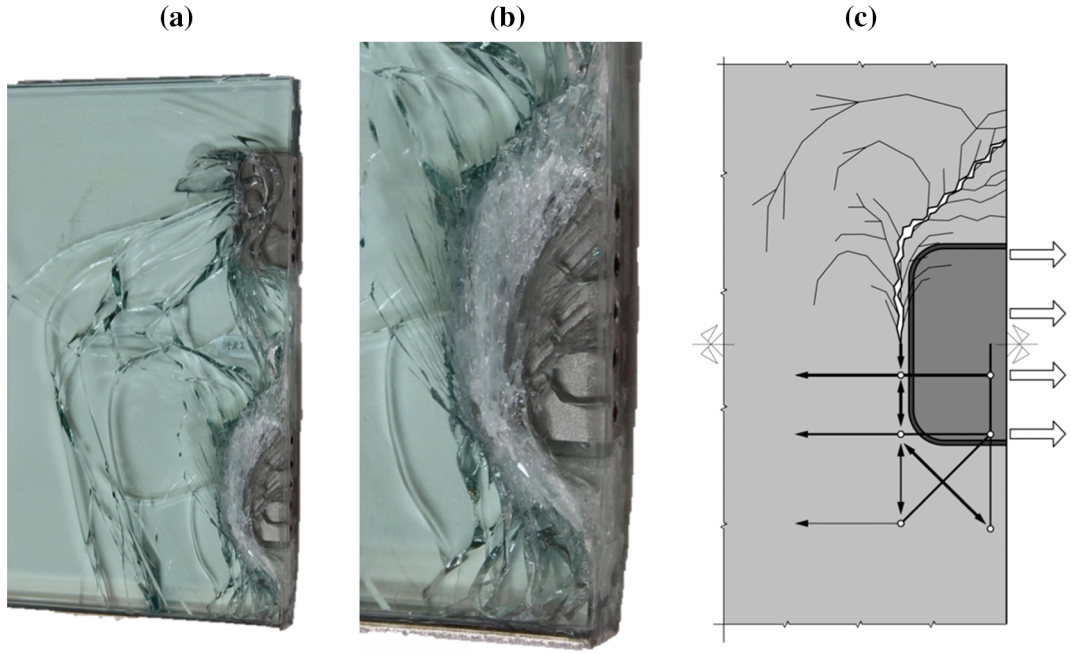

Fig. 19 **a** Photo of type A beam after monotonic test, **b** close view at bottom embedded connection and **c** scheme of the in-plane load transfer mechanism

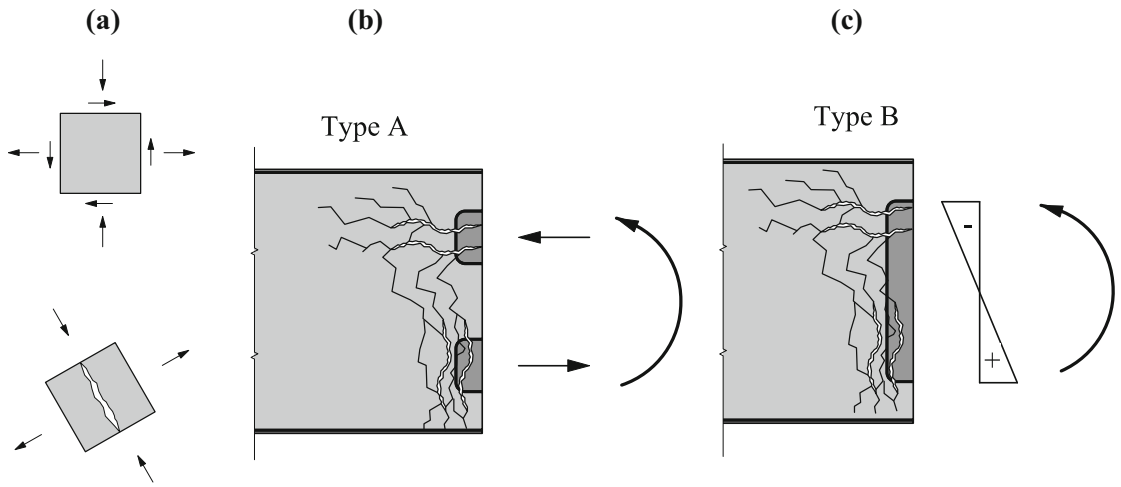

Fig. 20 **a** Scheme of the crack plane orientation with respect to principal stress directions, **b** expected cracks directions of type A beam and **c** expected cracks directions of type B beam

the frontal edge of the insert and at 45° direction at the two sides of the insert. This is in line with the experimental observation since Fig. 19b shows that glass cracks are concentrated (i) along the frontal edge of the metal insert and (ii) at the two sides of the metal insert with a 45 inclination.

The through-thickness behaviour instead can be described by Fig. 21a, which shows a cross-section scheme of the connection and an equilibrated strut-and-tie system. A static analysis of this scheme suggests that the most solicited tensile element is the one indicated by dashed line. According to that, it is therefore

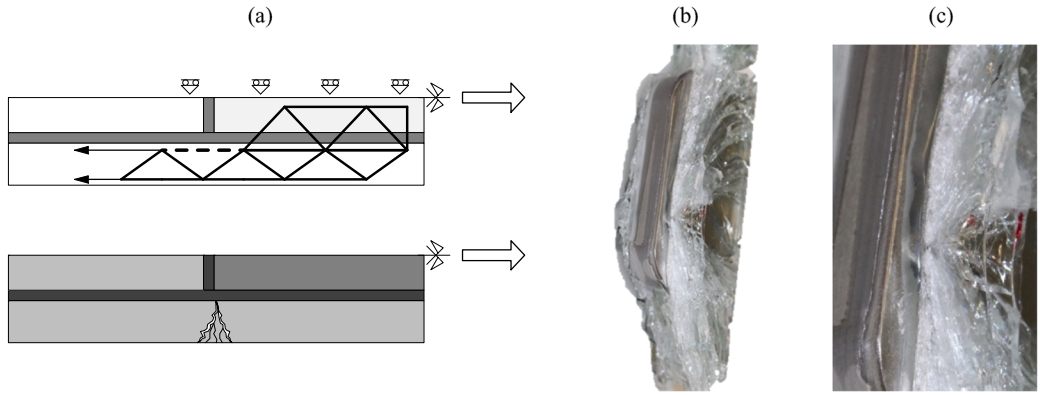

Fig. 21 **a** Scheme of the through-thickness load transfer mechanism, **b** photo of type A connection after monotonic test and **c** close view at crack initiation

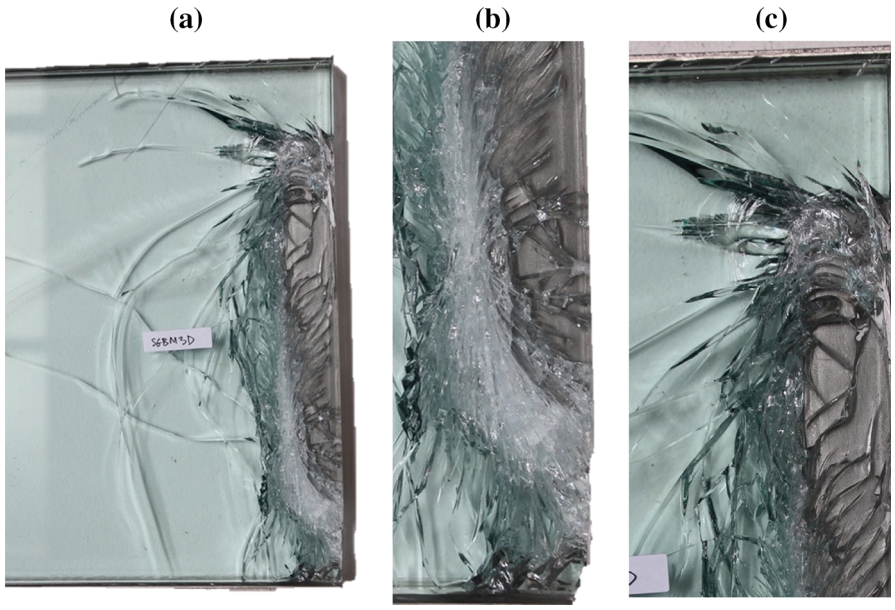

Fig. 22 **a** Photo of type B beam after monotonic test, **b** close view at the bottom of the embedded connection and **c** close view at the top of the embedded connection

expected that the crack is occurring in the internal face of the external glass layer. This is in line with experimental results since the crack initiation is observed to be located at the inner surface of the glass layer (see Fig. 21b, c). More detailed studies on the local mechanical behaviour of embedded can be found in (Santarsiero 2015) where small-scale tests of embedded connections are tested at different temperature and analysed with finite numerical analysis.

Considerations similar to type A beam can be made also on the fracture pattern of type B beam (see Fig. 22a). The crack pattern is vertically oriented at the bottom (Fig. 22b) and, towards the top of the connection, the cracks deflect and align along the horizontal direction (Fig. 22c). This fracture pattern confirm the above mentioned mechanical consideration.

5.1.2 Type C beams

The tests result shows that type C beam exhibits a different structural behaviour than type A and B. More specifically, if compared to type A and type B, type C beam shows a stress-wise efficient, redundant and ductile mechanical response.

Firstly, the experimental observation suggests that type C embedded connection might be more efficient than type A and B in transferring forces into the glass panel. The first crack seems to be not caused by the

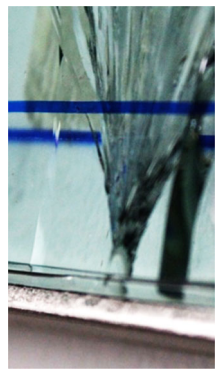

Fig. 23 Photo of the first crack in the glass at the bottom edge of type C beam during monotonic test

stress intensification occurring at the connection, but rather related to the maximum bending capacity of the beam. However, due to the large statistical spread of glass strength, more tests are necessary to further investigate this consideration. The first crack occurs at the bottom edge of the beam, far from the connections region, and it is characterized by a typical bending '*v-shape*' (see Fig. 23). More specifically, the crack starts at the bottom edge, and it propagates upwards splitting in several cracks, typical behaviour of cracks in glass component in bending (Louter et al. 2012a, b) (Fig. 24). With the increasing of load and displacement, more cracks occur in both beam segments (see Fig. 26, from a–d). These cracks are similar to the first one, i.e. located at the beam edge, far from connection region and characterized by a typical '*v-shape*' of bending cracks (see Fig. 27). The comparison of several cracks indicates that the beam reached its bending capacity, while the connection is still able to transfer load. In type C beam the connection is therefore not the critical element of the component as for type A, type B and the beam is able to reach its ultimate bending capacity.

The test also shows that each crack that occurs before the maximum load involves only one layer of glass and that the cracks are not overlapping each other (see cross section shown of Fig. 25a). This could explain why the stiffness of the beam is not affected by the cracks in the glass. When the cracks are not overlapping, the interlayer is able to 'bridge the glass crack, i.e. to transfer force by involving the un-cracked glass panels close to the crack, and therefore the global stiffness of the beam is preserved (Fig. 24).

When some of the cracks start to be overlapping, the load displacement curve shows a significant decrease in stiffness. This is because, where the cracks are overlapping, forces in the glass can be transferred only by the tearing of the interlayer (see white arrow, Fig. 25c).

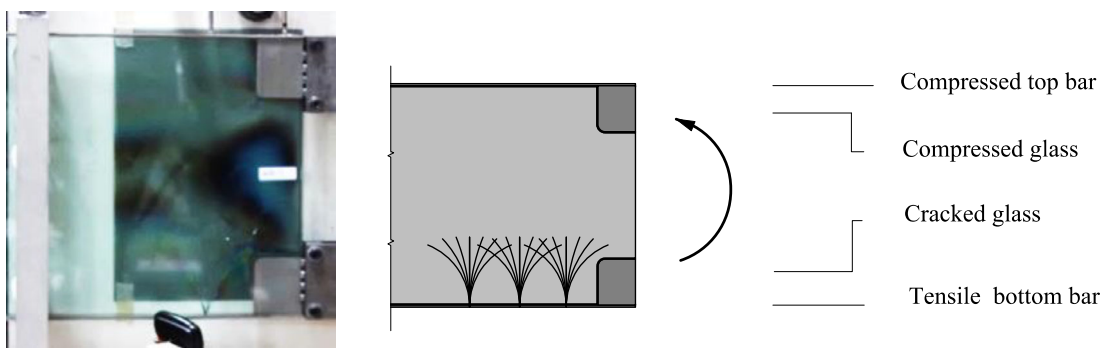

Fig. 24 **a** Photo of type C beam during monotonic test before maximum load and **b** scheme of the type C beam in cracked stage before maximum load

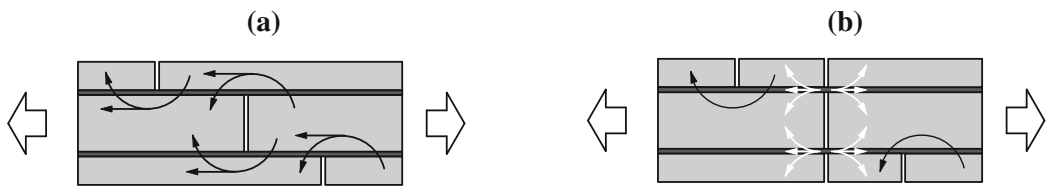

Fig. 25 Type C beam after glass breakages: plan section at bottom edge with **a** not overlapping cracks and **b** overlapping cracks

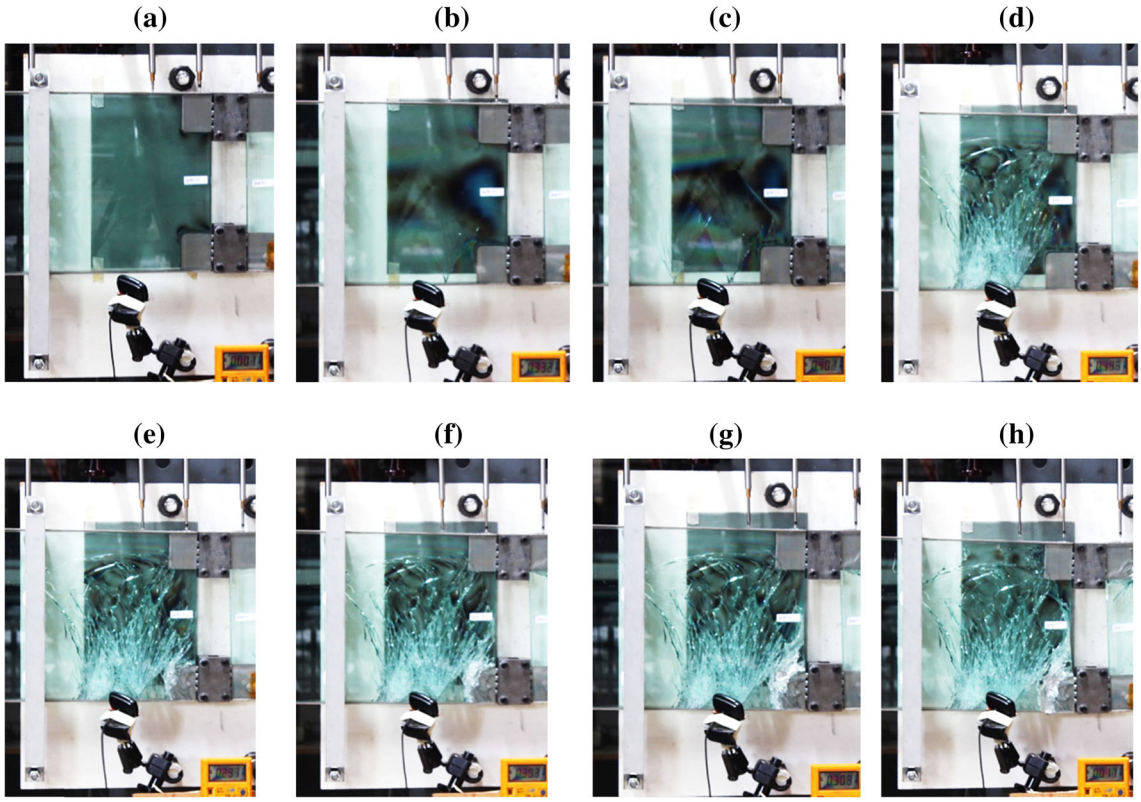

Fig. 26 Photos of type C beam during monotonic test

At this location, the mechanical response is therefore more compliant than before, which causes a significant reduction of stiffness in the beam. This is in line with the observation of (Louter et al. 2012a).

Previous tests on type A and B beam showed that their maximum load carrying capacity is limited by glass fracture. Indeed, after glass fracture, type A and B connections are not able to transfer further load between the two half beams. The test result of type C instead indicates a more redundant mechanical behaviour. The breakage of glass panels beam does not correspond to the failure of type C beam. More specifically, even in case of several cracks at the level of the connection (see Fig. 26e–g), the beam is still able to sustain the applied load. This is because the connection uses multiple load paths to transfer load between the two beam segments. Before glass breakage, the force applied to the metal insert can be transferred to the beam by (i) the adhesive at the frontal edge, (ii) the adhesive at top edge, (iii) the adhesive at the two lateral surfaces and (iv) the mechanical connection between the insert and the steel bar. The force redistribution between these items depends on their relative stiffness ratios.

Generally speaking, when a redundant system is used, the forces can be redistributed to other mechanisms of load transfer in the case of failure of one of the load paths. In this case, the force that was previously transferred by the adhesive is, after glass breakage, redistributed to the mechanical connection between insert and steel bar. The beam is therefore able to sustain to the applied bending moment, even after the occurrence of several cracks in the connection region. This redistribution of forces causes a reduction of the stiffness of the connection, thus of the beam (as shown by Fig. 7c), but prevents beam collapse. The beam is still able to carry 71 % of the maximum load and it is able to develop large deformation before ultimate failure of the beam. A quantitative comparison between type A, B and C beam is collected in Table 2.

It is then observed that type C beam exhibits a more ductile structural response than type A and B. Indeed, after the occurrence of several cracks in the glass, the

Fig. 27 Photo of glass cracks in type C beam during monotonic test

connection develops large deformation before breakage. This is because of the plastic deformation that occurs in the steel bar close to the metal insert (see Fig. 28). In that respect, it is important that the thickness of the steel reinforcement is neither too small nor too large. The first case would lead to steel plastification and breakage before the occurrence of several cracks in the glass. The second would lead to crushing or buckling of the top region of glass under compression stress field before steel plastification. An optimum design of the reinforcement bar in this case was 3 mm such as it would allow to develop several cracks in the glass and it would provide a ductile failure mode to the glass beam dominated by steel plastification.

The graph of Figs. 7c and 26 shows that the beam is able to sustain load even after the occurrence of several cracks. This indicates that type C beam shows a structural behaviour that is comparable to the one of reinforced concrete components. More specifically, when the glass is severely cracked, the bending moment is transferred by the tensile force at the bottom steel bar, by the compression force at the top steel bar and by the compressed glass part. According to that, the fracture pattern of glass plate is expected to show a transition region between tensile and compressive stresses. The crack pattern showed by Fig. 29 indicates that these considerations are in line with the experimental observation. The cracks start at the bottom and propagate vertically up to the beginning of the compression region (also called neutral axis). Also, in agreement with the previous consideration from solid mechanics, the cracks are initially vertically oriented and, when they approach the top edge of the beam, they curve towards horizontal direction. In this region, indeed, the glass is subjected to horizontal compressive forces and therefore the cracks are expected to be mainly oriented along horizontal direction.

5.2 Creep tests

In this and the following section, the normalized creep displacements are computed and presented by Fig. 30.

Table 2 Results of monotonic tests of type A–C beams

Type	Load at first crack (kN)	Displacement at first crack (mm)	Maximum load (kN)	Maximum displacement (mm)	Safety margin F_{max}/F_{crack} (–)	Ductility d_{max}/d_{crack} (–)
A	17.5	11.3	17.5	11.3	1.00	1.00
B	25.7	17.6	25.7	17.6	1.00	1.00
C	32.4	11.5	44.5	35.6	1.37	3.10

Fig. 28 Photos at the steel bar after monotonic test of type C beam

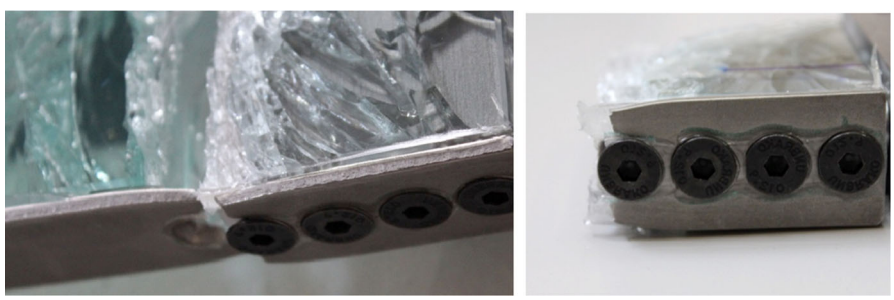

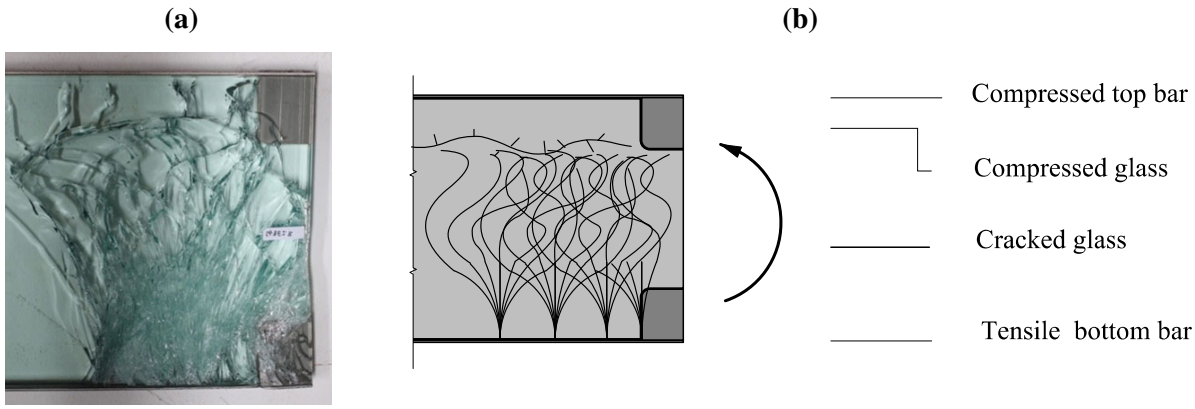

Fig. 29 **a** Photo of type C beam after monotonic test and **b** scheme of the type C beam in cracked stage

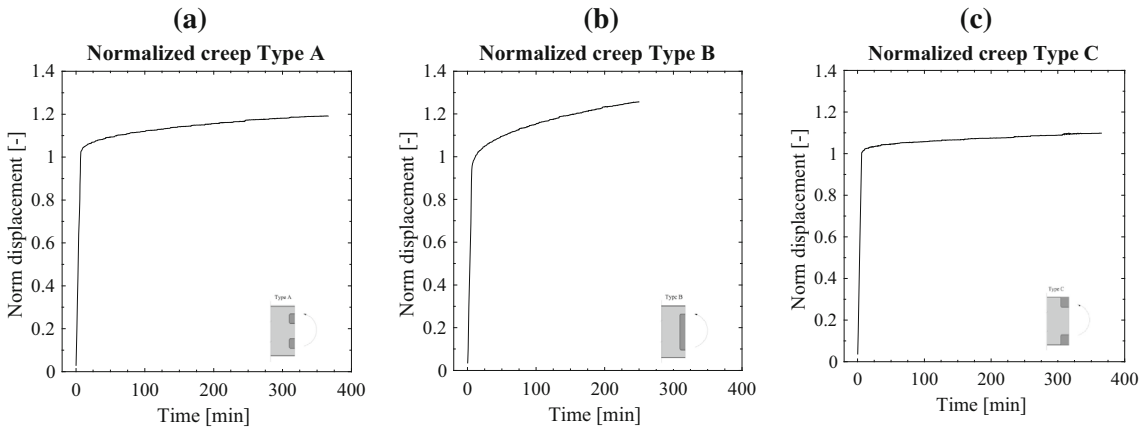

Fig. 30 Normalized displacement of creep tests **a** type A, **b** type B and **c** type C

This computation is done to allow for direct comparison, since the three types of beams have different connection geometry and different value of applied load. Normalized displacements are calculated dividing by the displacement value at the load application, here called initial displacement.

Figure 30a shows that the creep deformation of type A beam is about 30 % of the initial displacement. Type B beam instead, shows a creep deformation about 17 % of the initial displacement (see Fig. 30b). A possible interpretation to this difference could be the following. Type B connection is characterized by a larger bonded surface than type A. This means more adhesive area is involved to develop the bending moment necessary to equilibrate the applied load. The more pronounced visco-elastic behaviour of type B then might be associated to the larger area of SG involved in developing the moment at the connection level.

The creep deformation of type C beam is instead more limited than A and B. The creep deformation is about 10 % of the initial displacement. It is also observed that the gradient of the displacement-time curve reduces with time quicker than the other beams. The reduced creep displacement of type C beams is due to the redundancy that characterizes type C connection. Indeed, type C connection allows to activate multiple paths for the transfer of forces between the two beam segment. More specifically, in addition to the adhesive connection between metal insert and glass panel, the force is also transferred by the mechanical connection between the inserts and the steel bars. The global creep deformation of the beam type C is therefore reduced,

Table 3 Different stages of damage test protocol on type C beam under constant load of 15 kN

Stage	Damaged items	Location	Damage level
0	None	–	None
1	2/3 FT glass panels	Left beam segment	Full breakage
2	18 h creep		
3	HS glass panels	Right beam segment	Cracks at the short vertical edges
4	3/3 FT glass panels	Left beam segment	Full breakage
5	HS glass panels	Right beam segment	Further damage at several locations

Table 4 Effects of damage tests on type C beam under constant load

Stage	Damaged items	Increase of displacements between stages (%)
0	None	0
1	2/3 FT glass panels	16
2	18 h creep	32
2	HS glass panels	4
3	3/3 FT glass panels	22
4	HS glass panels	3

since the mechanical connection does not creep under constant load over time. An additional aspect should be considered. Due to the different breakage load, geometry and location of the metal inserts, the adhesive is subjected to different forces in type A B and C. This might also have an effect on the creep displacement over time.

It should be noticed that more test should be performed to confirm these consideration, since they are based on few preliminary investigations on three prototypes only. In addition,[3] given the different geometry and applied load, detailed numerical analysis should be performed to analyse and simulate the complex visco-elastic creep stress field distribution over time. This should be done by implementing in the numerical model the visco-elastic property of the adhesive material at the tested temperature.

5.3 Damage test

This test aims to simulate a scenario of vandalism damage to a type C beam and to investigate the effects of such damage to the beam when it is subjected to constant load over time. In order to maximise the effects of such inflicted damage, the beam is composed by a FT beam segment (left) and a HS beam segment (right). An overview of the test protocol is given by Table 3.

This test is divided in five stages: (i) the two external layers of the FT beam segment are firstly broken (ii) the beam is subjected to constant load over 18 h (iii) the HS half beam is damaged at the two short edges (iv) the last inner layer of the FT beam segment is broken and (v) further damage is induced to the right HS beam. The effects of each stage in terms of vertical displacement are summarized by following Table 4. The effects of damage at each stage are here discussed as increase of the vertical displacement in the center compared to the previous stage.

In the first stage, the breakage of the external layers of the fully tempered glass panels induces an increase of 16 % of vertical displacement, yet without failure of the beam (Fig. 31a).[4] This is because type C connection

[3] Also given the different level of load and bonded area.

[4] It is to notice that the breakage of both external layers does not initiate crack in the inner layer. This suggests that the internal shock wave due to the glass breakage does not generate stress intensification capable of initiating cracks in the inner layer.

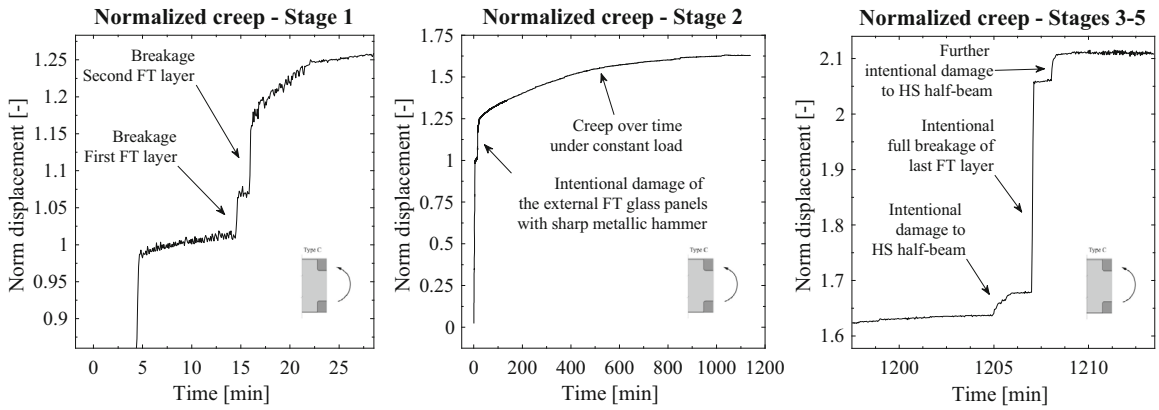

Fig. 31 Normalized creep displacement in type C beam during damage test. **a** Stage 1: breakage of the two external fully-tempered glass panels, **b** stage 2: creep under constant load for 18 h and **c** stage 3: damage to the right HS beam, stage 4: breakage of third inner layer of left FT left-half beam and stage 5: further damage of right HS beam segment

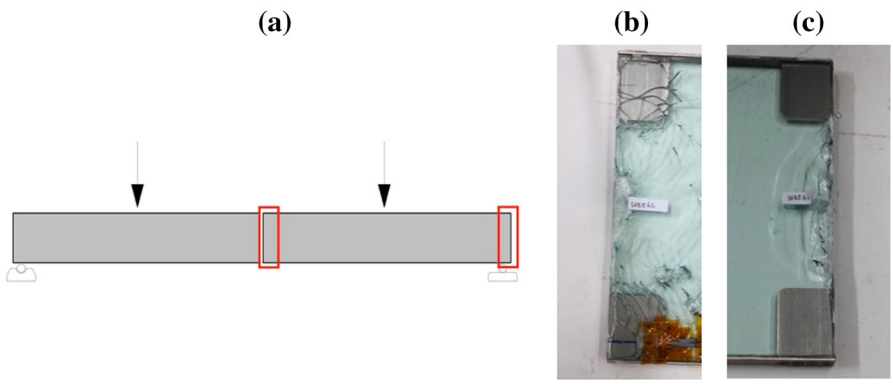

Fig. 32 Damage induced during stage 3 at the two vertical short edges of the HS glass panels **a** locations, **b** photo at central edge and **c** photo at right edge

is able to redistribute the forces from the adhesive to the mechanical component of type C connection. The connection is then able to involve the inner layer of glass in the mechanical response of the beam. Because of the activation of the inner layer of glass, the reduction of stiffness after breakage is limited. It should be noticed that in this test, due to the tempering residual stresses, the fracture is much more pronounced than previous monotonic tests of type C annealed beam. Then, Fig. 31 shows that, in stage two, type C beam is able to sustain constant load over time (18 h) with 2 out of 3 layer fully broken. The creep deformation after 18 h is observed to be about 32 % of the initial displacement (see Fig. 31b).

In the third stage, the right HS beam segment is intentionally damaged at the two vertical edges (see locations indicated in Fig. 32). Although a significant damage is dynamically induced to the glass component by hitting the beam with a sharp metallic hammer, the beam is able to sustain the applied load and minor effects are measured, i.e. only 4 % increase of displacement (see Fig. 31c).

In the fourth stage, when the only remaining inner glass layer of the FT beam segment is broken, a significant increase of displacement is measured (see Fig. 31c). More specifically the beam shows a further increase of 22 % of displacement. This is because the inner glass layer is now fully fragmented and it is not providing stiffness to the beam. However, the beam does not collapse and is capable to sustain the same applied load. This is because the applied bending moment can be transferred by a post-breakage mechanism composed by the bottom steel bar subjected to tensile force, the top steel bar subjected to compression and the fractured glass subjected to compressive force (see scheme of Fig. 33b). This scheme is also confirmed by a photo of the fracture pattern of the glass beam taken

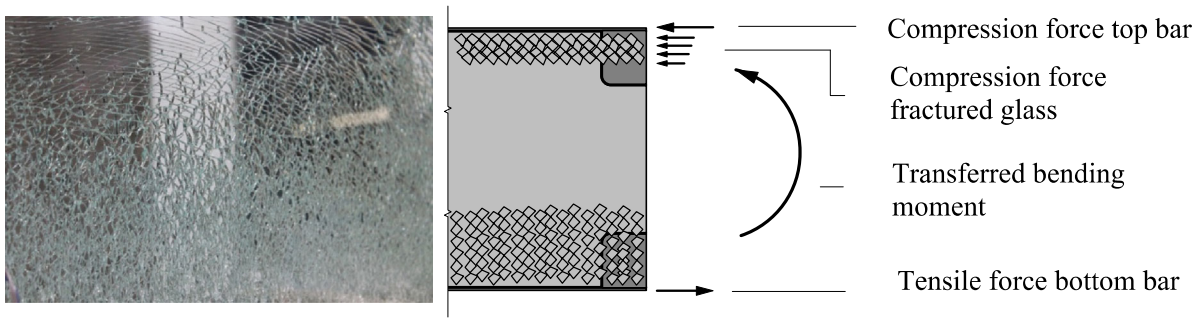

Fig. 33 **a** Photo of FT glass panel during damage test and **b** scheme of the mechanical response of type C beam in cracked stage

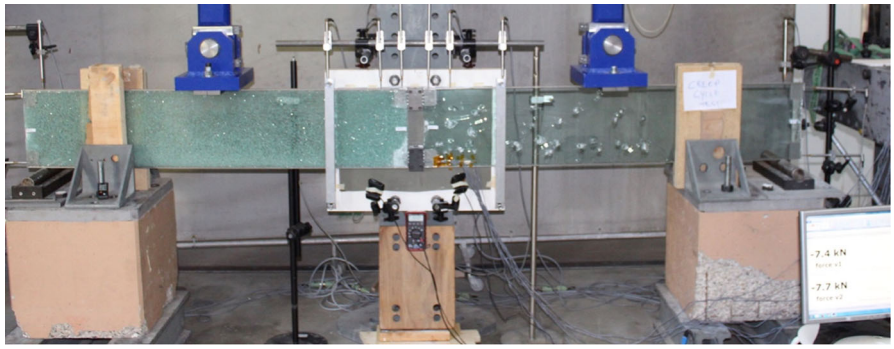

Fig. 34 Type C beam during damage test under constant load over time (15 kN)

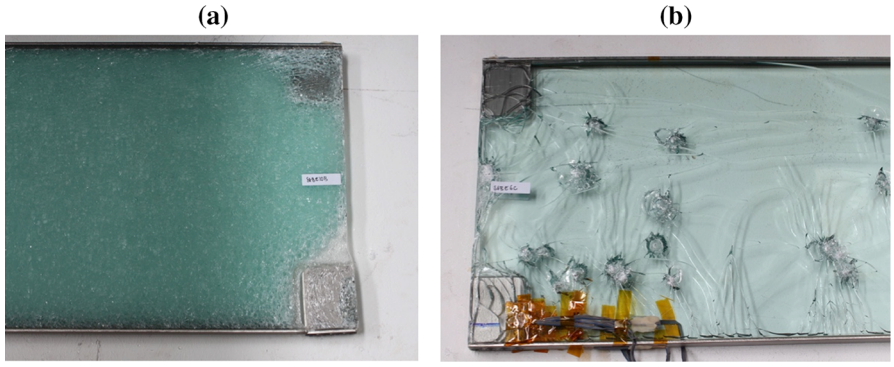

Fig. 35 Type C beam after damage test **a** left FT beam segment and **b** right HS beam segment

during the test (Fig. 33a). The fragmentation seems to follow vertical and horizontal direction respectively at the bottom and at the top. This is in agreement with the expected orientation of crack as a function of the direction of principal stresses as previously discussed.

In the last fifth stage of this test, further damage is induced to the HS half beams by hitting again the beam with a sharp hammer now at several locations along the beam (see Figs. 34 and 35b). After this further damage the beam is able to sustain the same applied load with an increase of displacement of 3 %.

From this section it is therefore concluded that type C beam, due to the redundancy of its connection, is able to resist severe damage scenarios at several locations and to sustain the applied load over time even in case of breakage of all glass panels. However, it should be noticed that more tests are necessary to confirm the considerations made in this section since they are based on one single test. For example, further tests and analysis should focus on the capability of SG to keep in place the small broken pieces of glass under sustained load over a longer period of time. In addition, due to the SG temperature-dependent behaviour, it is of interest to repeat test at high temperature, to evaluate the effects of an accidental damage scenario at high temperature.

6 Conclusion and outlook

In this work, a large-scale experimental study of laminated glass beams with embedded connections is presented. The mechanical behaviour of laminated glass beams is investigated under different loading scenario. Tests are performed under monotonic, creep and damage protocol. The beams are reinforced at top and bottom edges with stainless steel bars. Different geometries and locations of the embedded laminated adhesive connections are considered: type A (located at an intermediate position), type B (located in the centre) and type C beams (located at top and bottom edges and connected also to reinforcement bars). All embedded laminated connection are bonded to the glass panels with SentryGlas interlayer.

The results of monotonic tests showed that embedded connections represents an adequate means of load transfer for moment connections between glass beams. The ultimate load carrying capacity of type A and B beam is limited by glass breakage. A mechanical interpretation of the structural behaviour of these beams at the connections is presented, which is confirmed by the fracture pattern observed during the tests. Type C beam showed a more redundant and ductile response than type A and B. Firstly, it is observed that the first crack occurs far from the connection. This seems to indicate that in type C beam the connection might not represent, stress-wise, the critical element of the beam. However, given the large statistical variation of glass resistance, more tests are necessary to further study this aspect. Secondly, the test showed that even in case of several cracks, the beam is still able to sustain the applied load and to show large plastic deformation. The ultimate load bearing capacity is indeed limited by the ultimate plastic strain of the steel bar. The creep tests showed that type A and B beams exhibit creep deformation of 20 and 30 % when subjected to constant load over time. The creep of type C beam is smaller than type A and B (10 %). A final test is performed by inducing a diffuse damage to a type C beam under constant load over time. From this test is concluded that type C beam, due to the redundancy of its connection, is able to resist severe damage scenarios at several locations and to sustain the applied load over time even in case of breakage of all glass panels.

In conclusion, this study showed that structural connections between glass beams can be realized with embedded connections. More specifically, the choice of an appropriate geometry and design of the embedded connections can have substantial effects on the mechanical behaviour of the beam. In particular, the use of type C embedded connections allows to achieve a redundant and ductile structural behaviour.

Further work should focus on the analytical and numerical modelling of the tests in order to analyse the non-linear stress field distribution in the glass, to be compared for validation with the strain gauges measurements obtained during the tests. Further study and large-scale tests at different temperature should be performed to evaluate the effects of the SG temperature dependent behaviour.

Acknowledgements The authors would like to thank the Swiss National Science Foundation for founding the present research (Grants 200020_150152 and 200021_134507). In addition, the collaboration of the students Jordan Benoît, Elodie Vermot and Clara Schischlik is gratefully acknowledged. Finally, the COST Action TU0905 "Structural Glass – Novel Design Methods and Next Generation Products" is also acknowledged for facilitating the research network.

Compliance with ethical standards

Conflicts of interest On behalf of all authors, the corresponding author states that there is no conflict of interest.

Appendix 1: Strain gauges measurements

See Figs. 36, 37, 38 and 39.

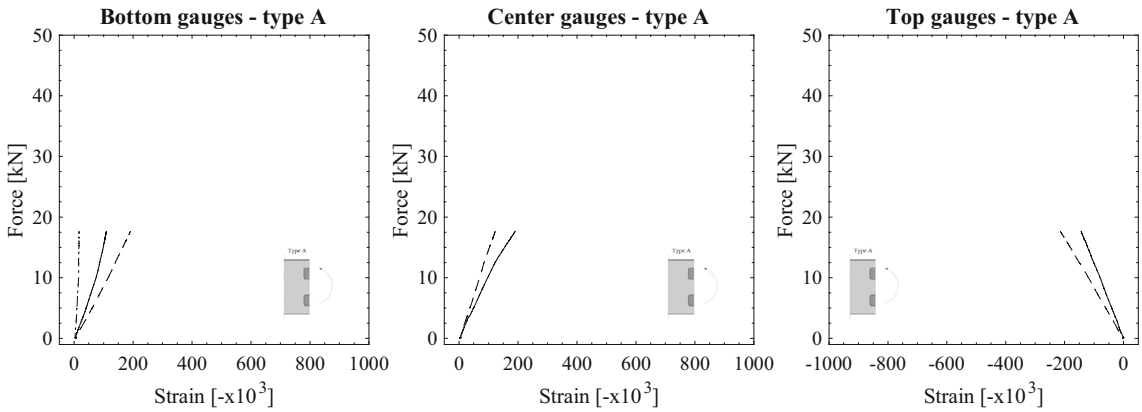

Fig. 36 Bottom, centre and top gauges of type A beam under monotonic test

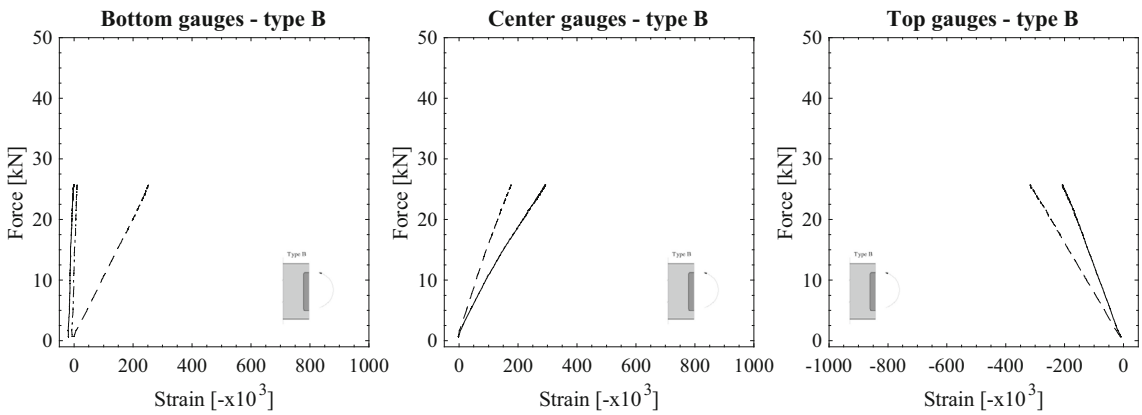

Fig. 37 Bottom, centre and top gauges of type B beam under monotonic test (two out of three bottom gauges did not work)

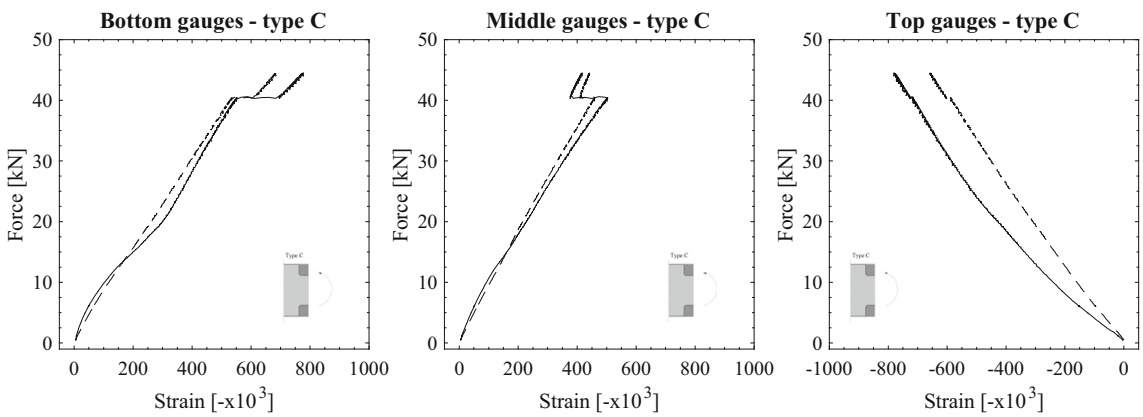

Fig. 38 Bottom, centre and top gauges of type A beam under monotonic test

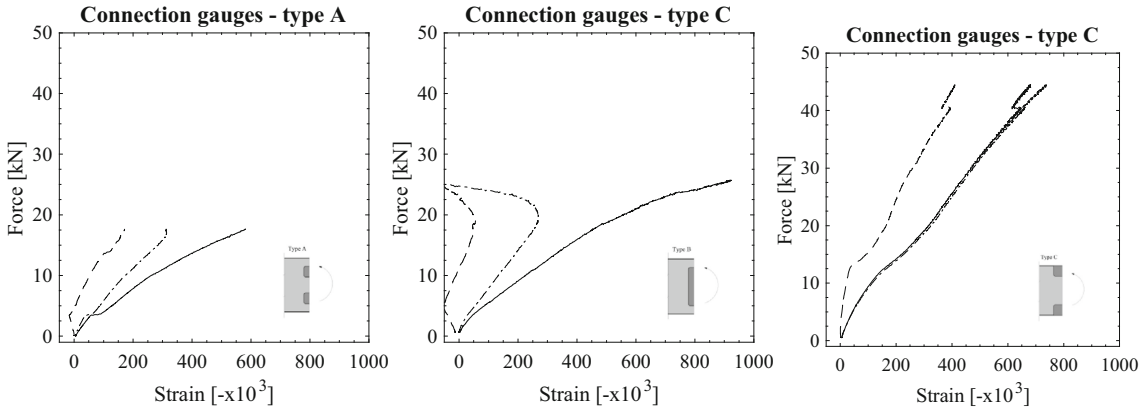

Fig. 39 Connection gauges for type A, type B and type C beams under monotonic test

References

Amadio, C., De Luca, O., Fedrigo, C., Fragiacomo, M., Sandri, C.: Experimental and numerical analysis of glass-to-steel joint. Struct. Eng. **134**(8), 1389–1397 (2008)

Baitinger, M.: Zur Bemessung von SL-belasteten Anschlüssen im konstruktiven Glasbau. Thesis Dissertation, RWTH Aachen (2009)

Belis, J., De Visscher, K., Callewaert, D., Van Impe, R.: Laminating metal-to-glass: preliminary results of case-study. In: Glass Performance Days (2009)

Belis, J., Van Hulle, A., Callewaert, D., Dispersyn, J.: Experimental investigation of unconventional canopy prototypes, suspended by adhesive bonds. In Challenging Glass 3. IOS Press, Delft (2012)

Beyer, J.: Ein Beitrag zum Bemessungskonzept für punktgestützte Glastafeln. Thesis Dissertation, Technischen Universität Darmstadt (2007)

Beyer, J., Seel, M.: Spannungsfaktoren für die Bemessung punktgestützter Verglasungen. Stahlbau **81**(9), 719–727 (2012). doi:10.1002/stab.201201601

Blandini, L.: Structural use of adhesives in glass shells. In: Challenging Glass. IOS Press, Delft (2010)

Carvalho, P., Cruz, P.J.S.: Connecting through reinforcement—experimental analysis of a glass connection using perforated steel plates. In: Challenging Glass 3. IOS Press, Delft (2012)

Carvalho, P., Cruz, P.J.S., Veer, F.: Perforated steel plate to laminated glass adhesive properties. In: Glass Performance Days (2011)

Dias, V., Hechler, O., Odenbreit, C.: Determination of adhesives properties for non-linear numerical simulation of structural steel-glass connections. In: Challenging Glass 3. IOS Press, Delft (2012)

Dispersyn, J., Belis, J.: Numerical research on stiff adhesive point-fixings between glass and metal under uniaxial load. Glass Struct. Eng. **1**(1), 115–130 (2016). doi:10.1007/s40940-016-0009-2

Dispersyn, J., Belis, J., Jaegher, J.De: Influence of corner and edge distance of adhesive point-fixings for glass structures. Eng. Struct. **105**, 174–185 (2015). doi:10.1016/j.engstruct.2015.09.037

Dispersyn, J., Belis, J., Sonck, D.: New glass design method for adhesive point-fixing applications. In: Proceedings of the ICE—Structures and Buildings (2015). doi:10.1680/stbu.13.00103

Dispersyn, J., Santarsiero, M., Belis, J., Louter, C.: A preliminary study of the nonlinearity of adhesive point-fixings in structural glass facades. J Facade Des Eng 2(1–2), 85–107 (2014)

Huveners, E.M.P., Van Herwijnen, F., Soetens, F., Hofmeyer, H.: Mechanical shear properties of adhesives. In: Glass Performance Days (2007)

Lenk, P., Lancaster, F.: Connections in structural glass. In: Glass Performance Days (2013)

Louter, C., Belis, J., Veer, F., Lebet, J.-P.: Durability of SG-laminated reinforced glass beams: Effects of temperature, thermal cycling, humidity and load-duration. Constr. Build. Mater. **27**(1), 280–292 (2012a). doi:10.1016/j.conbuildmat.2011.07.046

Louter, C., Belis, J., Veer, F., Lebet, J.-P.: Structural response of SG-laminated reinforced glass beams: experimental investigations on the effects of glass type, reinforcement percentage and beam size. Eng. Struct. **36**, 292–301 (2012b). doi:10.1016/j.engstruct.2011.12.016

Ludwig, J.: Tottenham Court Road Station—plaza entrances structures and building—structural glass. In: Challenging Glass 4 & COST Action TU0905 Final Conference (2014)

Ludwig, J.: Tottenham Court Road Station Upgrade—structural glass plazas. In: International Conference on Building Envelope Design and Technology (2015)

Maniatis, I.: Numerical and experimental investigations on the stress distribution of bolted glass connections under in-plane loads. Thesis Dissertation, Technische Universität München (2006)

Marinitsch, S., Schranz, C., Teich, M.: Folded plate structures made of glass laminates. In: Challenging Glass 4 & COST Action TU0905 Final Conference (2014)

Marinitsch, S., Schranz, C., Teich, M.: Folded plate structures made of glass laminates: a proposal for the structural assessment. Glass Struct Eng. (2015). doi:10.1007/s40940-015-0002-1

Martens, K., Caspeele, R., Belis, J.: Load-carrying behaviour of interrupted statically indeterminate reinforced laminated glass beams. Glass Struct. Eng. (2016). doi:10.1007/s40940-016-0017-2

Mocibob, D.: Glass panel under shear loading—use of glass envelopes in building stabilization. Thesis Dissertation, École Polytechnique Fédérale De Lausanne—EPFL (2008)

Mocibob, D., Belis, J.: Coupled experimental and numerical investigation of structural glass panels with small slenderness subjected to locally introduced axial compression. Eng. Struct. **32**(3), 753–761 (2010). doi:10.1016/j.engstruct.2009.12.003

O'Callaghan, J.: Thinking big with structural glass. In: Glass Performance Days (2009). doi:10.3233/978-1-60750-672-0-15

O'Callaghan, J., Coult, G.: An all glass cube in New York City. In: Glass Performance Days (2007)

Overend, M., Maniatis, I.: The influence of finite element modelling on the stress distribution in bolted glass connections. In: International Conference on Civil, Structural and Enviromental Engineering Computing (2007)

Overend, M., Nhamoinesu, S., Watson, J.: Structural performance of bolted connections and adhesively bonded joints in glass structures. J. Struct. Eng. **139**(12), 04013015 (2013). doi:10.1061/(ASCE)ST.1943-541X.0000748

Puller, K.: Untersuchung des Tragverhaltens von in die Zwischenschicht von Verbundglas integrierten Lasteinleitungselementen. Thesis Dissertation, University of Stuttgart (2012)

Puller, K., Sobek, W.: Load-carrying behaviour of metal inserts embedded in laminated glass. In: Challenging Glass 3. IOS Press, Delft (2012)

Puller, K., Denonville, J., Sobek, W.: An innovative glass connection technique using an ionomer interlayer. In: Glass Performance Days (2011)

Santarsiero, M.: Laminated connections for structural glass applications. Thesis Dissertation, École Polytechnique Fédérale De Lausanne—EPFL (2015). doi:10.5075/epfl-thesis-6828

Santarsiero, M., Louter, C.: Embedded and point laminated adhesive connections for glass structures: parametric non-linear numerical investigations. In: Glass Performance Days, pp. 265–273 (2013)

Santarsiero, M., Carvalho, P., Louter, C., Cruz, P.J.S.: Experimental and numerical investigations of metal-to-glass embedded connections with thin stainless steel plate. In: COST Action TU0905, Mid-term Conference on Structural Glass. Taylor & Francis Group, Porec (2013a)

Santarsiero, M., Louter, C., Lebet, J.: Parametric numerical investigation of adhesive laminated point connections. In: COST Action TU0905, Mid-term Conference on Structural Glass. Taylor & Francis Group, Porec (2013b)

Santarsiero, M., Louter, C., Lebet, J.-P.: The mechanical behavior of SentryGlas and TSSA laminated polymers in cured and uncured state in uniaxial tensile test. In: Challenging Glass 4 & COST Action TU0905 Final Conference, pp. 375–384 (2014). doi:10.1201/b16499-55

Schneider, J., Franz, J.: Classification of the material properties of interlayers for laminated glass regarding the post-breakage behavior. In: Engineered Transparency (2012)

Siebert, G., Herrmann, T.: Glazing with countersunk point fittings. In: Challenging Glass 3 (2010)

Silvestru, V.A., Englhardt, O.: Application study for hybrid adhesively bonded glass-steel façade elements. In: Challenging Glass 4 & COST Action TU0905 Final Conference (2014)

Vogt, I.: Strukturelle Klebungen mit UV- und lichthärtenden Acrylaten. Thesis Dissertation, Technical University of Dresen (2009)

Watson, J.: Premature Failure in UV-Cured Adhesive Joints. In: ISAAG (2010)

Watson, J., Nielsen, J., Overend, M.: A critical flaw size approach for predicting the strength of bolted glass connections. Eng. Struct. **57**, 87–99 (2013). doi:10.1016/j.engstruct.2013.07.026

Weller, B., Nicklisch, F., Vogt, I.: Loadbearing tests on bonded glass frame corners bonded glass frames. In: IABSE-IASS Symposium (2011)

Weller, B., Nicklisch, F., Prautzsch, V., Vogt, I.: Outline of testing and evaluation program used in selection of adhesives for transparent adhesive joints in all-glass load-bearing structures. J. ASTM Int. **9**(4), 104088 (2012). doi:10.1520/JAI104088